Link Quality Modeling for LoRa Networks in Orchards

Kang Yang*
University of California, Merced.
Merced, California, USA

Yuning Chen*
University of California, Merced.
Merced, California, USA

Xuanren Chen
University of California, Merced.
Merced, California, USA

Wan Du
University of California, Merced.
Merced, California, USA

ABSTRACT

LoRa networks have been deployed in many orchards for environmental monitoring and crop management. An accurate propagation model is essential for efficiently deploying a LoRa network in orchards, e.g., determining gateway coverage and sensor placement. Although some propagation models have been studied for LoRa networks, they are not suitable for orchard environments, because they do not consider the shadowing effect on wireless propagation caused by the ground and tree canopies. This paper presents *FLog*, a propagation model for LoRa signals in orchard environments. *FLog* leverages a unique feature of orchards, i.e., all trees have similar shapes and are planted regularly in space. We develop a 3D model of the orchards. Once we have the location of a sensor and a gateway, we know the mediums that the wireless signal traverse. Based on this knowledge, we generate the First Fresnel Zone (FFZ) between the sender and the receiver. The intrinsic path loss exponents (PLE) of all mediums can be combined into a classic Log-Normal Shadowing model in the FFZ. Extensive experiments in almond orchards show that *FLog* reduces the link quality estimation error by 42.7% and improves gateway coverage estimation accuracy by 70.3%, compared with a widely-used propagation model.

CCS CONCEPTS

• **Networks** → **Wide area networks**; *Network measurement*.

KEYWORDS

Low-Power Wide-Area Networks, LoRa, Link quality, Signal propagation model, First Fresnel Zone

---

*Both authors contributed equally to this research.

1 INTRODUCTION

Orchard crops are a significant contributor to the economy in California, generating over 8.96 billion dollars in profit in 2021 [45]. Smart orchard management, such as smart irrigation [11], tree health monitoring [9] and pest control [35], is crucial for improving yield and minimizing cost [25]. All these applications need to deploy a large number of sensors across the orchards, e.g., tens or even hundreds of acres. LoRa is a promising solution with a communication range of several miles, allowing gateways to receive sensor data in a large field [7, 15, 18, 26, 33, 42, 47, 48, 55]. However, this range is only achievable in free space [6, 17], which is rarely found in orchards.

Our preliminary experimental results reveal that in an almond orchard, LoRa signals can only be reliably transmitted up to 140 m with a Spreading Factor (SF) of 10; whereas LoRa signals with the same hardware and transmission parameters can reach a communication distance of 2 km in free space. In orchards, nodes are typically installed close to the ground, under the tree canopy. Meanwhile, LoRa gateways are often placed on towers of 6-10 m because there are no high buildings on farms and it is expensive to construct taller towers. As a result, the energy of wireless signals may be absorbed and reflected by the ground, which can affect the LoRa signal propagation. In addition, the wireless signal from a sensor node must penetrate through the canopies of multiple trees to reach a gateway, which is installed on a tower higher than the trees.

In this paper, we study the propagation modeling problem of LoRa signals in orchard environments, which require estimating the attenuation of wireless signals as they propagate through all mediums between the transmitter and the receiver, such as air and tree canopy. Although two propagation models [10, 29] for LoRa have been developed for large-scale urban scenarios, they cannot be used in orchards. For example, for a sensor node in orchards, its signal propagation varies significantly across different directions, since the signal traverses different distances in canopies. In addition, several foliage propagation models [4, 19, 46] have been studied for wireless signals passing through trees. They are developed for high-frequency channels (*e.g.*, 5 GHz in satellite communications) but are not applicable to LoRa links. The propagation characteristics of low-frequency LoRa signals are different from high-frequency signals, and these foliage propagation models do not consider the impact of the ground on LoRa signal propagation.

To study the characteristics of LoRa signal propagation in orchards, we conduct a series of experiments using a gateway and a LoRa sensor node. The node is deployed at different locations for experiments (Section 4.1 for the detailed description of the experiment setting). Based on our experimental results, we made three

observations. 1) If the send and the receiver are both under trees, the link quality of a line-of-sight (LoS) path is worse than that of non-line-of-sight (NLoS) paths. When a wireless signal passes through a tree, it may penetrate, scatter (*i.e.*, reflected or refracted), or diffract around the tree. This power loss is known as the shadowing effect, which needs to be analyzed from a 3D perspective. 2) Due to the long wavelength of LoRa signals, wireless signals can easily diffract from tree trunks and branches. 3) The low installation height of LoRa sensor nodes means that the ground has an apparent shadowing impact on wireless signal propagation.

Based on the observations above, this paper presents *FLog*, a wireless signal propagation model designed for LoRa links in orchards. It is inspired by the regular layout of orchards, where all trees are perfectly aligned and have a similar shape and canopy density, as they are planted and pruned at the same time. The shape of a tree can be modeled by a few parameters, including tree height, trunk height, and canopy width. The layout of an orchard can be modeled by the shape of trees, the distance between adjacent rows, and the distance between adjacent trees.

Given the locations of a sensor node and a gateway, we can leverage our 3D orchard model to study the shadowing effect that the wireless signal will experience from the sensor node to the gateway. Based on the shadowing effect analysis, our wireless propagation model can calculate the attenuation that the signal will have as it travels through the air and tree canopies. Combining the predefined transmission settings, including antenna gains and transmission power, we can calculate the strength of the received LoRa signal.

FLog adopts the First Fresnel Zone (FFZ) to capture the complex shadowing effect caused by tree canopies and the ground in orchards. The FFZ is a 3D ellipsoid region with two focus points located at the sensor node and the gateway. This zone carries most of the signal energy received by the receiver. Different links have their unique portions of the wireless transmission medium in their FFZ. To calculate the portion of each medium for a transmission pair, we perform numerical sampling in the FFZ. Each sampling point may encounter free space, trees, or the ground. The portions of sampling points in each medium over the total number of points are used as weights for profiling the shadowing effect. These weights are used to combine the intrinsic path loss exponent (PLE) of each transmission medium, resulting in the final PLE of the classic Log-Normal Shadowing model in the FFZ.

Besides the weights, we also need to determine the PLEs for each medium in *FLog*. We obtain these parameters by fitting the collected data using a nonlinear least square algorithm [39]. We adapt these parameters according to environmental variation based on a few recently received packets.

To demonstrate the applications of our propagation model, we use *FLog* to determine gateway coverage. A LoRa node is considered to be covered by a gateway if the Packet Delivery Ratio (PDR) exceeds 80% [53, 56]. The PDR is computed using a BER model [14], with inputs of Signal-to-Noise Ratio (SNR) and SF. We use *FLog* to estimate the SNR for any LoRa nodes and a gateway, and thus the coverage of that gateway under different transmission settings.

Extensive experiments have been conducted in two almond orchards and one walnut orchard. The results show that *FLog* can reduce path loss estimation errors by up to 42.7% compared to the Log-Normal Shadowing model. Additionally, *FLog* provides more

accurate PDR estimation for gateway coverage, reducing the estimation error by 70.3% compared to the Log-Normal Shadowing model. Numerical analysis shows that *FLog* can facilitate scheduling fewer gateways while maintaining reliable link quality.

In summary, this paper makes three major contributions:

- We study the propagation modeling problem of wireless LoRa signals in orchards. It is essential to deploy LoRa networks for smart orchard management.
- We propose ourSystem, a novel propagation model for LoRa networks in orchards. It leverages the regular tree layout of orchards to model the complex shadowing effect caused by tree canopies and the ground.
- Extensive experiments demonstrate the effectiveness of *FLog*. A gateway coverage study shows the usability of *FLog*.

2 BACKGROUND AND MOTIVATION

After a brief introduction of some basic LoRa concepts and the Log-Normal Shadowing model, we conduct experiments to study LoRa links in free space and orchards.

2.1 LoRa Networks

LoRa physical layer uses Chirp Spread Spectrum (CSS) modulation, enabling long-distance and low-power communication [16, 51].

Frequency Band. LoRa operates on license-free radio frequency bands, such as 915 MHz in North America. It can transmit over long distances of several miles or more in rural areas. In contrast, high-frequency bands such as 2.4 GHz or 5 GHz used by WiFi have a short communication range, typically limited up to 45 m indoors [12, 49]. This short communication distance makes it difficult to provide coverage for orchards that span several acres.

Expected Signal Power (ESP). LoRa defines ESP to quantify the received signal strength [10, 28, 29], which is derived from the RSSI (Received Signal Strength Indicator) and SNR:

$$\text{ESP} = \text{RSSI} + \text{SNR} - 10 \cdot \log_{10}\left(1 + 10^{0.1\text{SNR}}\right) \tag{1}$$

where the unit of ESP and RSSI is dBm and the unit of SNR is dB. RSSI and SNR are reported from the LoRa gateway for each packet.

2.2 Log-Normal Shadowing Model

The Log-Normal Shadowing model is widely used to predict the received signal power [37]. The ESP of a received packet, P_{rx}, is calculated as follows [37].

$$P_{rx} = P_{tx} + G_{tx} + G_{rx} - PL \tag{2}$$

where P_{tx} represents the transmission power in dBm, G_{tx} and G_{rx} denote the transmitting and receiving antenna gains in dBi, respectively. The last term PL is the path loss in dB and can be calculated using the Log-Normal Shadowing model [37]:

$$PL(d) = \overline{PL}(d_0) + 10 \cdot n \cdot \log\left(\frac{d}{d_0}\right) + X_\sigma \tag{3}$$

where the distance between a LoRa node and a gateway is denoted as d in meters, n is PLE, and X_σ is a zero-mean Gaussian distribution with a standard deviation of σ. The reference path loss $\overline{PL}(d_0)$ is obtained from field measurements at a reference distance of d_0,

(a) Free space scenario   (b) A typical scenario in orchards   (c) Sensor nodes at 7 directions to the gateway   (d) Gateway example
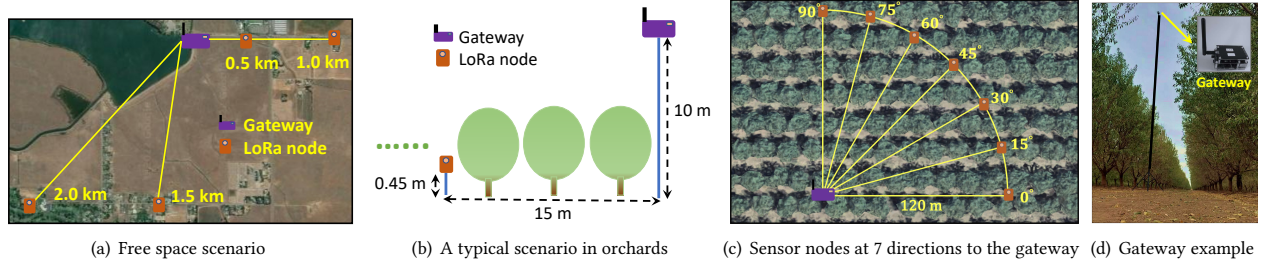
Figure 1: The deployment layout of the almond orchard and illustration for different directions.

(a) Free space scenario   (b) A typical scenario in orchards
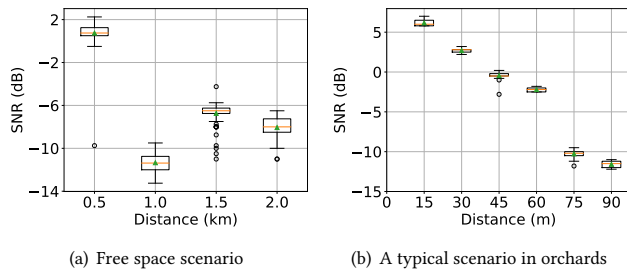
Figure 2: The measured link quality (SNR) in the free space and almond orchard for different communication distances.

(a) Distance = 80 m   (b) Distance = 120 m

Figure 3: The measured link quality (ESP) at different directions for two communication distances.

where d_0 is normally set to 1 m [10]. Based on our collected packets, we obtained an average $\overline{PL}(d_0)$ of 78.59 dBm.

2.3 Free Space Scenario

We conducted an experiment to measure the quality of LoRa links in free space. Figure 1(a) shows that a LoRa node is placed at four locations with communication distances of 0.5, 1.0, 1.5, and 2 km. The nodes and gateway are installed on two poles with heights of 6 m and 10 m respectively. During the experiment, the nodes transmitted packets periodically with SF10, $P_{tx} = 14$ dBm, a bandwidth of 125 kHz, and a coding rate of 4/5.

Figure 2(a) depicts the experiment results. Even at a distance of 1.5 km, the link's SNR remains above the receiving sensitivity threshold (*i.e.*,-7.5 dB for SF7). This indicates that LoRa nodes can transmit packets using SF7 at distances of up to 1.5 km in free space. However, the SNR at a distance of 1.0 km is lower than that at 1.5 and 2.0 km, primarily because buildings and trees obstruct the propagation path, as illustrated in Figure 1(a). This highlights the significant impact of blockages on link quality.

2.4 Orchard Scenario

Figure 1(c) depicts an almond orchard where trees are organized tidily to facilitate uniform allocation of sunlight, water, and soil nutrients. LoRa nodes and the gateway are deployed in orchards as shown in Figure 1(b). The nodes are typically positioned on the ground or attached to the main branches, measuring data related to soil and tree health. The installation height is usually between the ground and the canopy, less than 1.2 m (*e.g.*, 0.45 m in our implementation). Meanwhile, the gateway is mounted on top of a pole or tower, providing long communication coverage, as shown

in Figure 1(d). Therefore, the signals from sensor nodes normally pass through two mediums: free space and trees in orchards.

2.4.1 Short Communication Distance. We conducted an investigation of link quality in an almond orchard, as depicted in Figure 1(b). Our measurements of the SNR were taken from 15 m to 90 m, with 3 to 14 rows of trees between the sensor and gateway, and the transmission settings were identical to those outlined in Section 2.3. From Figure 2(b), we observed a significant reduction in communication: at only 90 m, the SNR was -12.0 dB. As a result, SF10 was necessary for a reliable communication distance of 90 m. Conversely, SF7 was suitable for distances of 1.5 km in free space. By fitting our collected data, we found that the PLE in the almond orchard was 2.95. This value is larger than that of free space, indicating a shorter communication distance, and reflects the high path loss in the orchard caused by tree blockage.

2.4.2 Large Deviation at Different Directions. We then measured the received signal strength in seven directions, ranging from 0° to 90° in 15° increments for a fixed distance, as depicted in Figure 1(c). Figure 3 shows the ESP of the received signal at different directions for communication distances of 80 m and 120 m. The dotted red line represents the average ESP in seven directions for one distance. The results indicate a significant variation in the signal ESP across different directions, with discrepancies of up to 13 dBm, such as -105 dBm versus -118 dBm at 0 degrees and 45 degrees.

According to Equation 3, the Log-Normal Shadowing model can only predict one value for a given distance, as shown by the black line in Figure 3. Although the predicted ESP with the Log-Normal Shadowing model is close to the average ESP, with errors of less than 1 dBm, the overall ESP error across all the collected data can exceed 4 dBm due to the significant deviation in signal strength
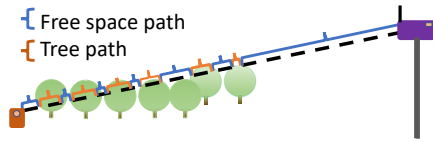
Figure 4: The illustration of the strawman solution.

(a) Experimental Settings   (b) ESP for four locations

Figure 5: Comparison between LoS and NLoS settings.

across different directions. This finding motivates us to develop a new propagation loss model that can account for the variation in signal strength across different directions.

3 STRAWMAN SOLUTION

In this section, we explore a strawman solution to model link quality in orchards. We first build a 3D profile for an orchard. Using this profile, we specify the PLE in a Log-Normal Shadowing model.

3.1 3D Modeling of Orchards

Abstracting One Tree. Botanists have developed several detailed tree models based on physiological knowledge [41]. However, these models require precise measurements of the shapes of trunks, branches, and leaves for all trees in an orchard, which is a labor-intensive process. We adopt a simple solution proposed by Torrico *et al.* [43]. It profiles the trunk as a cylinder and abstracts the crown as an ellipsoid with varying horizontal and vertical radii, as shown in Figure 1(b). To create a profile of a tree, we need to measure its height, trunk height, canopy width, and trunk radius.

Abstracting an Orchard. Orchards typically have a uniform layout, with trees being planted at the same time of year and exhibiting similar shapes. To analyze an orchard, we adopt a Cartesian coordinate system with the x-axis and y-axis representing the directions along and across rows, respectively. We also measure the distances between adjacent rows and adjacent trees in one row, which determine the positions of all trees in the Cartesian coordinate system.

Therefore, by adding just two parameters, we can extend tree modeling to orchard modeling. With all of these parameters as input, we can reconstruct the orchard as 3D shapes, which can be translated into point clouds. Specifically, given the position of any point, we can determine whether it falls within the foliage or not.

3.2 Adapting PLE with Line Shadowing

Figure 4 depicts the signal propagation path between a LoRa node and a gateway, where the path is viewed as a direct line. The path includes both free space and foliage portions, which can have different shadowing effects on the signals. Therefore, it is intuitive to consider these two parts separately.

To achieve this, we calculate the free space and foliage portions along the propagation path's direct line, denoted as P_{open} and $P_{foliage}$, respectively. To calculate the foliage portion $P_{foliage}$, we equally split the direct line into numerous points. If a point is in the tree, then the foliage points increase by 1; otherwise, the free space points increase by 1. Finally, the foliage portion $P_{foliage}$ is obtained by dividing the foliage points by the total number of points, which is similar to the free space portion calculation. The sum of these portions should be equal to one.
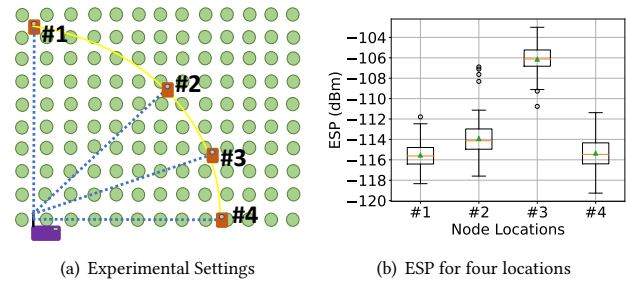
As free space and foliage have different shadowing effects, they have different PLEs in the Log-Normal Shadowing model. To account for this heterogeneity, we propose an adaptive PLE calculation approach. This involves separating the path into two types of media (free space and foliage) and then recombining them together.

$$PLE_{comb} = P_{open} \cdot \alpha + P_{foliage} \cdot \beta \qquad (4)$$

where α is the free space PLE and β is the PLE when the space is filled with foliage. To determine the values of α and β, we perform a least square fitting on a collected dataset. The final PLE_{comb} is a compromise between the two values. For example, if $P_{open} = 1$, it means that no trees are present and the path can be treated as free space. Once we have determined the PLE_{comb}, we can calculate the total path loss using the Log-Normal Shadowing model.

From experimental results in Figure 13(c), the strawman solution (marked as "LLog" in the figure) can provide different estimations in different directions, but this model underestimates or overestimates the path loss in some directions. The possible reason is that we modeled the propagation path as a direct line. We only consider the shadowing effect in the direct line, but the surrounding area also plays a role in the signal propagation path.

4 THE DESIGN OF *FLOG*

This section presents a theoretical analysis of the LoRa signal propagation in orchards and makes three key observations. We then introduce a path loss model based on the FFZ theory.

4.1 Analysis of LoRa Signal Propagation

To accurately design a path loss model for orchards, it is crucial to understand how the signal propagates within this environment. Therefore, we conducted three preliminary experiments to investigate the LoRa signal propagation characteristics in orchards.

4.1.1 Line-of-Sight Path Signal Strength. Typically, LoS paths are expected to experience significantly lower propagation loss than NLoS paths at the same distance [27]. In order to validate whether this assumption holds true for the LoRa signal in orchards, we conducted a series of controlled experiments.

Figure 5(a) shows the experimental setup where a gateway is positioned at the lower-left corner, and four different locations are selected to place LoRa nodes in varying directions but with the same communication distance of 60 m between the gateway and nodes. The gateway and nodes are placed at a height of 0.45m.

(a) Experimental Settings

(b) ESP for three settings
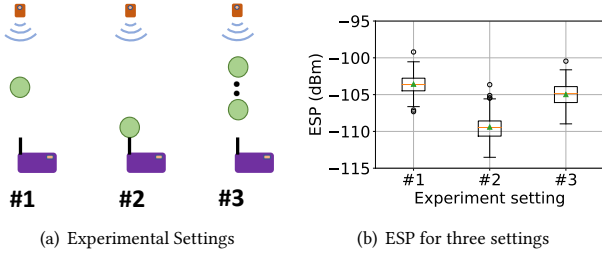
Figure 6: The diffracted signal strength.

(a) Experimental Settings

(b) ESP for three settings

Figure 7: The effect of ground absorption.

Locations #1 and #2 have a clear LoS propagation path, while locations #3 and #4 have an NLoS path that passes through two and ten trunks, respectively. At each location, a LoRa node transmits packets periodically for three minutes with an interval of 1.5 s.

According to Figure 5(b), location #3 with the NLoS path achieves the highest ESP, which is even higher than the LoS path (*i.e.*, location #1 and #2). Furthermore, despite having ten trunks in location #4, this NLoS path still attains a comparable ESP to the LoS settings at locations #1 and #2. In summary, we conclude that:

Observation 1: *For LoRa propagation in orchards, the LoS path does not guarantee a low propagation loss.*

4.1.2 Diffracted Signal Strength. Diffraction refers to the propagation of waves behind an obstruction. We conducted controlled experiments to evaluate the significance of the diffracted waves.

Figure 6(a) shows the setup of experiments, where the green circles represent tree trunks. In both settings #1 and #2, there is one trunk located between the nodes and the gateway. The difference is that in setting #2, the trunk is positioned very close to the gateway antenna, resulting in significantly weaker diffracted waves [31, 52].

Although setting #3 has five trunks between the gateway and node, resulting in weaker penetrating signal power, Figure 6(b) shows that its signal power is similar to that of setting #1. We can also see that setting #2 exhibits the lowest signal strength, with a difference of more than 6 dBm compared to setting #1 and 4 dBm compared to setting #3. This leads us to the second observation:

Observation 2: *Comparing setting #1 with #2, diffraction plays a crucial role in LoRa signal propagation. Comparing setting #1 with #3, the signal power from diffraction outweighs the power transmitted in the direct line.*

4.1.3 Ground Absorption. Signal propagation in orchards can be impacted by the low height of nodes, resulting in the absorption of signal energy by the ground. To investigate this effect on signal power, we conducted experiments in a free sand region without any obstacles. The experiments involved fixing the horizontal distance at 100 m and maintaining the sensor height at 0.45 m while varying the gateway height to 0.5 m, 1 m, and 1.5 m, as illustrated in Figure 7(a). The results, shown in Figure 7(b), reveal that increasing the gateway height leads to an increase in the received signal power.

Observation 3: *When the sender and receiver are in close proximity to the ground, a significant portion of the signal power can be absorbed by the ground.*

All of these observations demonstrate that the link quality can be influenced by the surrounding objects, and the "path" cannot be considered as simply the direct line between the sender and receiver.
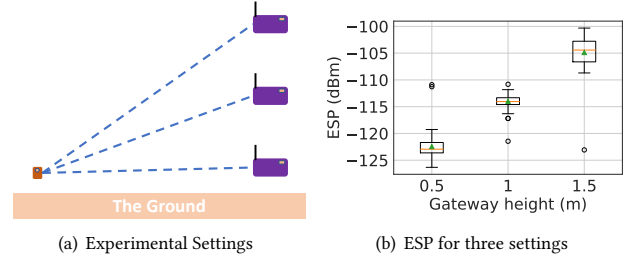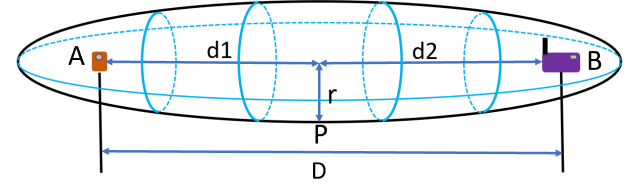
Figure 8: The illustration of FFZ.

Instead, more attention should be given to the surrounding regions along the signal propagation path when estimating path loss. To address this issue, we propose the use of FFZ theory in path loss calculations, as it takes into account the surrounding environment.

4.2 First Fresnel Zone for LoRa

The FFZ refers to the 3D ellipsoid region around the direct path through which the received signal passes. Figure 8 illustrates that a point P lies on the surface of the FFZ if and only if:

$$\sqrt{d_1^2 + r^2} + \sqrt{d_2^2 + r^2} = (d_1 + d_2) + \frac{\lambda}{2} \qquad (5)$$

where λ refers to the wavelength. This equation quantifies confocal prolate ellipsoidal-shaped regions with the sender and receiver located at two focal points. This theory suggests that all media within the FFZ shadows signals, not just media along direct path.

Based on Equation 5, the volume of the FFZ increases proportionally with wavelength. LoRa operates on the unlicensed frequency band of 902 MHz in America, which is much lower than other wireless technologies like 802.11 on 2.4 GHz, and 5 GHz. Therefore, the FFZ for LoRa is typically large. For instance, at a distance of 100m, the maximum radius of the FFZ could be more than 2.8m. This highlights the need to quantify the shadowing of the surrounding area, rather than solely relying on the direct path in LoRa.

4.3 *FLog* Design

In this section, we provide the details of *FLog*, including PLE calculation, media portion quantification, and parameters fitting.

4.3.1 PLE Calculation. Except for the foliage and free space, we also need to consider the ground shadowing effect. Because the FFZ of the LoRa signal has intersections with the ground due to the low height of sensor nodes. Therefore, we update PLE calculation Equation (4) as follows:

$$PLE_{comb} = P_{open} \cdot \alpha + P_{foliage} \cdot \beta + P_{ground} \cdot \gamma \qquad (6)$$

where two new variables, P_{ground} and γ, are introduced to represent the ground shadowing effect. The values of α, β, and γ correspond to the PLEs when the wireless signal propagates through free space, foliage, and ground, respectively. The portion of free space, foliage, and ground in the FFZ is denoted by P_{open}, $P_{foliage}$, and P_{ground}, respectively. The final PLE_{comb} in the FFZ is obtained as a weighted combination of α, β, and γ, where the corresponding weights are P_{open}, $P_{foliage}$, and P_{ground}. In an orchard, all the pairs of senders and receivers share the same α, β, and γ, but have different final PLE_{comb} due to the varying combination weights. The next two subsections explain how to determine the values of these six parameters.

4.3.2 Media Portion Quantification. The weights of each media in an FFZ are calculated by computing the volume of each media and dividing it by the total volume of the FFZ. However, computing this volume requires solving a triple integral in a constrained 3D space, which is computationally intensive and time-consuming. In this paper, we used a sampling approach by dividing the FFZ into multiple planes with equal spacing. Each plane was then further sampled into numerous points.

Specifically, we incremented the number of corresponding media points by one if a sampling point was located within that media. For example, if a sampling point was in free space, we incremented the free space points by one. The portion of each media was then calculated by dividing the number of points contained in that media by the total number of points in the FFZ. Therefore, the sum of the portions for all three media types should be one.

Sampling Planes. The first sampling plane is located at $d_0 = 1\ m$, which is the reference distance in the Log-Normal Shadowing model. The remaining sampling planes are equally spaced at an interval of p_gap. We empirically set $p\_gap = 0.25\ m$.

The number of sampling points in each plane varies and is proportional to the signal energy in the plane, which is calculated by multiplying the power flux density by the area of the plane. The radius of the plane can be determined via Equation 5. The power flux density of a sampling plane decreases proportionally to the square of the distance [37], *i.e.*, $4\pi d^2$, indicating that the number of sampling points in each plane should similarly decrease with distance. Therefore, the total number of sampling points on a plane i is given by $N_{plane}^i = N_{ref} \cdot S_i / 4\pi d_i^2$, where N_{ref} is a constant that can be adjusted to control the total number of sampling points, S_i is the area of plane i, and d_i is the distance between the sender and the plane i.

Sampling Points in a Plane. A sampling plane i contains N_{plane}^i sampling points. To determine the locations of these points in the plane, we first locate the central point of the plane, which serves as the first sampling point. We then divide the plane into multiple circles with varying radii, each centered at the central point. At each circle, we sample N_{sample} points with equal arc length. Due to the diffraction loss, the power flux density of the received signal is greater at the center of the plane than at the edges [31, 52]. we accordingly set the radii of the circles to increase quadratically from the central point to the edge of the plane.

4.3.3 Media PLE Fitting. To calculate the final PLE_{comb} in Equation (6), we also need to determine the values of α, β, and γ. The process for obtaining these values is outlined below.

Since soil properties typically remain stable in orchards, we assume that γ is constant. To determine its value, we utilized non-foliage data from Figure 7 and applied the least square algorithm to Equation (6), where $P_{foliage} = 0$ and $\alpha = 2$. This yielded a value of $\gamma = 5.39$, which will serve as the default for the remainder of the paper unless otherwise noted.

To determine the values of parameters α and β, we collected packets at multiple pairs of transceivers in our testbed, as described in Section 5.1.4. For each pair, we calculated three portions: P_{open}, $P_{foliage}$, and P_{ground}. We then combined Equations (1), (2), and (3) to obtain the final PLE_{comb}, using the RSSI and SNR values obtained after receiving a packet. Thus, the only unknown variables in Equation (6) were α and β. We then employed a least square error fitting algorithm to determine the optimal values of α and β.

4.3.4 Parameter Adaptation Mechanism. The parameters in Equation (6) may change along with the environmental dynamics, which can be categorized into four scenarios:

(1) Short-term environmental noise variation.
(2) **Transient weather changes**, *e.g.*, temperature or precipitation.
(3) **Foliage density changes** on a yearly cycle due to the growth and loss of leaves and fruits.
(4) **Long-term foliage shape changes.** The shape of foliage changes as the trunk and branches grow over several years.

To mitigate the impact of dynamic (1), we collect multiple packets to compute the average signal power as the reference signal power at a given location. Environmental dynamics (2) and (3) can affect α and β in Equation (6). We use the N most recently received packets from all sensor nodes to calibrate these two parameters. When a new packet is received, we obtain its measured ESP. The ESPs of the past N packets from M nodes will form $N \times M$ equations to calibrate α and β, as shown in the example equations below (where $i = 1, 2, \ldots, N$ and $j = 1, 2, \ldots, M$):

$$\begin{cases} PLE_1^1 = P_{\text{open}_1} \cdot \alpha + P_{\text{foliage}_1} \cdot \beta + P_{\text{ground}_1} \cdot \gamma \\ \qquad\qquad\qquad\vdots \\ PLE_j^i = P_{\text{open}_j} \cdot \alpha + P_{\text{foliage}_j} \cdot \beta + P_{\text{ground}_j} \cdot \gamma \\ \qquad\qquad\qquad\vdots \\ PLE_M^N = P_{\text{open}_M} \cdot \alpha + P_{\text{foliage}_M} \cdot \beta + P_{\text{ground}_M} \cdot \gamma \end{cases} \tag{7}$$

The new α and β could be fitted by employing the non-linear least square algorithm on the set of equations shown above. We empirically set $N = 5$. Note that all links in an orchard at the same cycle share the same α, and β.

Dynamic (4) refers to changes in the 3D profile of the orchard, which affect P_{open} and $P_{foliage}$ in Equation (6) for all nodes, but not α and β. To handle this dynamic, it is necessary to remeasure the tree height, trunk height, and canopy width to rebuild the 3D profiles. This is expected to be done every year or even longer.

4.4 Workflow of *FLog*

The farmer provides input parameters for generating the 3D orchard, and *FLog* estimates the link quality between any two locations in the orchard based on these parameters. The user can choose a configuration that they think is best suited for their orchard. Specifically, *FLog* requires the following parameters from the user: tree profile, layout, and deployment parameters.

(1) Tree Parameters: Tree height, trunk height, and canopy width: They are used to build the 3D profile of a single tree. As the growth accumulates, the user may measure these parameters every year or longer.

(2) Layout Parameters: The distances between adjacent rows and adjacent trees in one row are required for the layout configuration. These factors will never change. Sometimes there might be several blank positions for removed dead trees. *FLog* also accepts such input or updates.

(3) Sensor and gateway position (optional): If the application requirements dictate the placement of the sensor and gateway, the user should input their designated positions. Or we can determine the optimal position based on our *FLog* model.

Using the parameters outlined above, *FLog* creates an FFZ between any two locations in orchards. It then calculates the portion of foliage, free space, and the ground within this zone and estimates the link quality via Equations (2), (3), and (6). Additionally, *FLog* utilizes a parameter resetting mechanism to tune our model's parameters, which adapts to different environmental dynamics.

4.5 Applications of *FLog*

FLog can be used to deploy and operate a LoRa network in orchards, e.g., determining gateway coverage, sensor placement, and network resource allocation. We use gateway coverage as an example to demonstrate the application of *FLog* in a LoRa network deployment.

4.5.1 Gateway Coverage Estimation Application. Our path loss model can estimate gateway coverage by determining if a gateway can cover a specific location. Specifically, if the Packet Delivery Ratio (PDR) exceeds 80%, a gateway could cover a given location [53, 56]. Thus, our path loss model can estimate the PDR prior to deploying LoRa networks.

Packet Delivery Ratio. PDR can be estimated by the Bit Error Ratio (BER) and packet size, which is calculated as follows:

$$PDR = (1 - BER)^{8 \cdot S_p} \tag{8}$$

where S_p is the packet size in bytes, *e.g.*, 8 bytes in our implementation; the BER calculation is provided in [36]. **Signal-to-Noise Ratio.** Equation (1) can be used to calculate the SNR if the ESP and RSSI are known. Our path loss model can predict the ESP for any pair of nodes and gateway. Additionally, we calculate the received RSSI by averaging all collected data. In this way, we can compute the expected SNR as follows:

$$SNR = 10 \cdot \log_{10} \frac{1}{10^{\frac{RSSI - ESP}{10}} - 1} \tag{9}$$

In Section 5.4, we will compare the predicted gateway coverage using three path loss propagation models when SF = 7.

4.5.2 Benefits for Farmers. We will use the example of gateway coverage estimation to analyze the benefits for farmers offered by *FLog*. If the estimated propagation path loss is greater than the actual value, more gateways will be required than necessary, leading to an increase in gateway building costs. Conversely, if the estimated path loss is less than the actual value, some nodes may not be able to connect with gateways, rendering the sensor network incomplete and unsuitable for practical applications. Thus, an inaccurate model can significantly impact the efficiency and effectiveness of the sensor network. In Section 5.4, we quantify the benefits using real measurements in a specific orchard.

4.5.3 Other Application Scenarios. Theoretically, *FLog* could be utilized in wild forests or urban areas as long as an accurate 3D model can be generated and the portion of each medium can be obtained. However, trees in forests are irregularly placed and differ in species, age, and shape, making it highly labor-intensive and impractical to survey and map them all. Moreover, urban buildings are constructed using different materials and have varying PLEs. Additionally, large smooth surfaces on buildings create mirroring reflections, resulting in reflection-based multipath being the major component, which is different from the orchards. Future work could explore ways to adapt our model to wild forests and urban areas in a lightweight manner.

5 EVALUATION

We evaluate the overall performance of *FLog* in Section 5.2, Then, we investigate the performance under different factors in Section 5.3, followed by the performance on the application study in Section 5.4.

5.1 Experiment Setting

5.1.1 Hardware Implementation. LoRa nodes are hand-crafted with SX1276 Radio [2] on the Arduino Uno host boards [3]. They are equipped with a 3,000 mAh power bank. They work in the frequency band 904.3 MHz. The gateway executes a thread of LoRa Packet Logger [1] that demodulates packets and stores them as comma-separated values (CSV) files. Our model is implemented with Python on a PC with an Intel(R) Core (TM) i9-11900KF @ 3.50 GHz CPU with 16 cores.

5.1.2 Benchmarks. We compare the performance of *FLog* with the following two baselines.

- *Log-Normal Shadowing Model [37]*. It is calculated by Equation 3. We use the collected data to fit PLE in the orchard scenario. It is referred to as "Log".
- *Line-based Log-Normal Shadowing Model*. It is our strawman solution, which is introduced in Section 3. We call it "LLog".

5.1.3 Performance Criteria. The prediction accuracy of models is quantified by errors between the predicted ESP and the corresponding actual value for each packet. The unit of errors is dBm.

$$ESP \ error = (y_i - \hat{y}_i) \tag{10}$$

where y_i is the measured ESP for the i-th received packet and $\hat{y}_i$ is the predicted value.

5.1.4 Experiments in an Almond Orchard. We chose almond orchards as the main focus of our evaluation since they are a critical

agriculture industry in the US. In 2021, the US produced 2.5 billion pounds of almonds, with a value of over 7 billion dollars [44]. Moreover, the estimated almond acreage in California was 1.64 million acres, making it the largest producer of almonds in the world [44]. We also tested *FLog* in a walnut orchard, which is another dominant arbor crop worldwide.

Figure 9 shows locations of LoRa nodes and a gateway in an almond orchard with a size of $200 \times 200 \ m^2$. In this orchard, trees are planted in lines with a distance of 4.88 m, and lines are separated by 6.66 m. The almond trees are 6.1 m in height and 2.8m in width on average. The heights of the LoRa node and the gateway are set as 0.45 m and 10 m. Transmitting and receiving antenna gains (G_{tx}, G_{rx}) are 5 dBi and 3 dBi, respectively. The transmission power is 14 dBm, SF is 10, bandwidth is 125 kHz, and coding rate is 4/5.

5.1.5   Datasets. We measure the received packets at a large number of locations in an orchard. We also conduct experiments at some locations for months.

Spatial Dimension Dataset. As shown in Figure 9, the gateway is located in the lower-left corner of one of the 90-degree fan-shaped areas of the orchard. We have deployed LoRa nodes at 56 locations across this fan-shaped area to collect packets. For each received packet, we calculate the ESP by using its RSSI and SNR. The nodes are placed at communication distances ranging from 20 m to 160 m, with a step size of 20 m. We measured seven directions ranging from 0 to 90 degrees, with a step size of 15 degrees. At each location, the nodes transmit an 8-byte packet to the gateway every 1.5 seconds for a duration of 1.5 minutes. The experiment was conducted for a duration of 10 hours in the autumn of 2022, and 2900 packets were collected in total.

Temporal Dimension Dataset. Four LoRa nodes are deployed at four locations randomly selected from Figure 9 to collect data over four weeks in the spring (January and February 2023). We collected data continuously for 24 hours each week, resulting in a dataset of 69,173 packets. The dataset contains three environmental dynamics: (1) Short-term environment variations. (2) Transient weather changes, including temperatures ranging from 26.2 to 65.5°F and precipitation ranging from 0 to 0.15 inch/hour. (3) Foliage density changes. In the final week of the four-week period, almond trees started to bloom with flowers. By combining this with the spatial dimension data, foliage density can be classified into three categories: trees with dense leaves, trees without leaves, and trees with flowers. The long-term foliage shape changing (Dynamic 4) was emulated by collecting data in another almond orchard, where the almond trees have a height of 4.5 m and width of 2.6 m, which are different from the trees in the prior experiments.

Fitting and Testing Data. In the spatial dimension dataset, we used measurements collected from four randomly selected distances to fit the parameters in our path loss models, such as α and β. These measurements are referred to as fitting data. The data from the remaining four communication distances were used as testing data. To obtain the optimal parameter values on the fitting data, we employed the least square approximation method. These parameters were then used to estimate the link quality on the testing data.
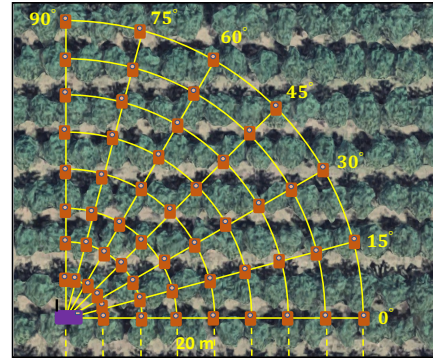
Figure 9: The testbed layout in an almond orchard.

5.2   Overall Performance

We evaluated the performance of *FLog* and benchmarks on both spatial and temporal dimension data.

5.2.1   Spatial Dimension. In the fitting and testing data, four communication distances were randomly selected from eight distances in our testbed. Therefore, there are $\binom{8}{4} = 70$ combinations to select the fitting and testing data. For each set of fitting data, we obtained corresponding fitted values of α and β. After analyzing all 70 combinations, we found that the mean value of α was 1.98 with a standard deviation of 0.11, while the mean value of β was 5.07 with a standard deviation of 0.17. We report all the estimation errors for these 70 combinations in Figure 10(b).

The ratio between the fitting data and testing data is 4:4, based on the number of communication distances. We also evaluated our model with ratios of 5:3 and 6:2. The settings of 5:3 and 6:2 had a similar performance to the ratio of 4:4, with a negligible difference in average estimation error of 0.09 dBm and 0.04 dBm. Therefore, we only report the results for the ratio of 4:4.

Communication Distance. Figure 10(a) presents the estimated curves of Log with changing communication distances. We do not draw the curve of the LLog and *FLog* because they have different estimated values in different directions for a given distance, while the Log model has only one value for each distance. Figure 10(b) quantifies the estimation error for different models in the CDF curve (cumulative distribution function). The average error of *FLog* is only 2.85 dBm, showing substantial performance improvement over other models in terms of link quality estimation. In particular, *FLog* decreases the ESP estimation error of Log and LLog by 42.7% and 35.2%, respectively. This is because Log does not consider the influence of direction on the received signal power and can only estimate the received signal power based on the communication distance in Equation 3.

Although LLog is aware of the ESP variation in different directions, it only considers the obstacle of lines between the LoRa node and gateway. However, the signal is concentrated in the FFZ based on the diffraction theory [37] and our preliminary experiments in Section 4. Therefore, *FLog* developed a more reasonable model to consider the shadowing effects in the FFZ.

Direction. Figures 10(c-d) present the fitted curves of all models and the estimation errors with different directions at a horizontal distance of 60m. It is observed that Log is unaware of directions

(a) ESP *vs.* distance   (b) ESP error (All distances and directions)   (c) ESP *vs.* direction (60 m)   (d) ESP error (All directions at 60 m)
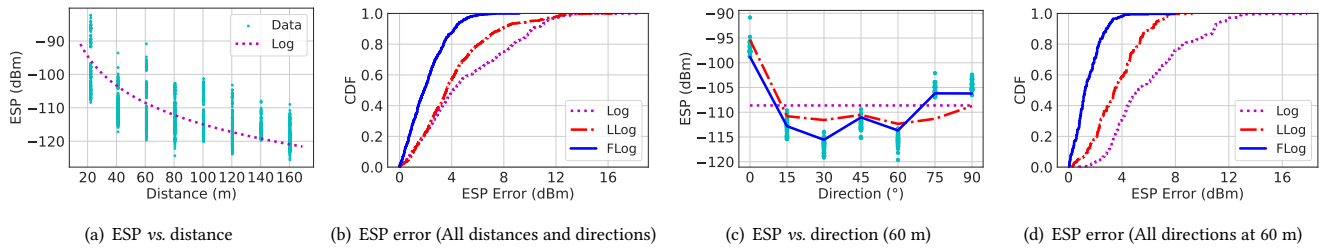
Figure 10: The overall performance of three models for different communication distances and directions. Figure (a) does not draw the fitted curve of the LLog and *FLog*, it is because they have different estimated values at different directions for one communication distance. Figure (c) plots the estimated value in different directions when the horizontal distance between LoRa nodes and the gateway is 60 m. The curve of the Log model is a horizontal line, which could not handle the direction.

Table 1: The ESP estimation error for three path loss models.

Models	Weissberger	ITU-R	COST235	O-H
ESP Error (dBm)	41.6	111.2	87.4	12.7

and thus provides a horizontal line as the estimated curve, which remains unchanged for different directions. Although LLog considers the influence of direction, it produces unstable performance. At direction 75°, LLog produces the largest error, that is, 5.93 dBm. This is due to the fact that LLog considers only the shadowing in the line of the propagation path, which results in overestimating or underestimating the ESP of the received signal. *FLog* considers all the shadowing in FFZ and jointly calculates them.

Empirical Foliage Loss Models. Table 1 presents the average estimation ESP error on the test data for four different foliage loss models, including Weissberger [46], ITU-R [4], COST235 [19], and Okumura-Hata models [10]. As we can see, these foliage models provide the lowest prediction accuracy compared with the Log, LLog, and *FLog* models. There are three main reasons for this.

Firstly, the above foliage loss models are developed using different wireless signals, such as WiFi. However, different wireless signals have different attenuation on the same foliage since the wavelength is different. Thus, the empirical models cannot be directly applied to our scenarios. Secondly, these loss models have no adjustable parameters to adapt to different scenarios. However, the Log-Normal Shadowing model can adapt to various situations by fitting its parameters, such as PLE. Hence, it can perform well if we fit it with the collected data on the specific case, compared with those path loss models with fixed parameters. Thirdly, those models cannot handle the ESP deviation in different directions. This is similar to the Log-Normal Shadowing model. They can only consider the effect of the communication distance on the signal strength, but not on other factors such as direction and surrounding trees.

5.2.2 Temporal Dimension. We use the temporal dimension data to test the models' performance on the three different environmental dynamics. We apply our parameter resetting mechanism to all path loss models, which uses the most recently received packets to calibrate models' parameters. Note that the environmental dynamic (1) was addressed by averaging the received ESP of multiple packets.

Environmental Dynamic (2): transient weather changes. We first obtain the temperature and precipitation from a weather

(a) ESP error *vs.* temperature   (b) ESP error *vs.* precipitation
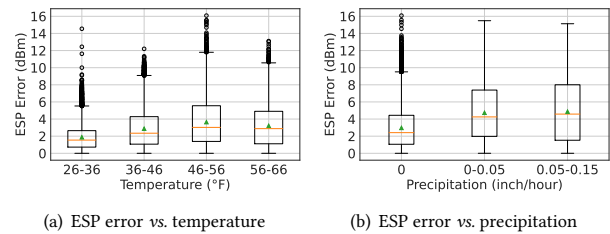
Figure 11: The impact of the environmental dynamic (2): transient weather changes.

station [40]. Next, we group the data based on the corresponding temperature and precipitation at the time of collection. Figure 11 illustrates that all the models can benefit from the parameter resetting mechanism. Specifically, models achieve no increased ESP prediction error for different temperatures and precipitation levels. Our system, *FLog*, still on average outperforms Log and LLog by 39.8% and 41.5% for different temperatures respectively. The experimental results show that *FLog* consistently outperforms the baseline models, Log and LLog, for different temperatures. This indicates the effectiveness of our parameter resetting mechanism in adapting to dynamic (2). This is reasonable because the proposed mechanism can adjust the values of parameters α and β based on the recently received packets. We analyzed the received ESP of LoRa signals under different temperature and precipitation conditions. Our findings indicated that the difference in signal power at different temperatures or precipitations was small. This small difference may be attributed to the effects of atmospheric and vapor molecules on electromagnetic waves, which become more apparent at frequencies exceeding 10 GHz. However, the absorbance for 900 MHz bands at short distances (< 50 km) is negligible [30].

Environmental Dynamic (3): foliage density changes. In the spatial and temporal dimension dataset, foliage density has three statuses: trees with dense leaves, trees without leaves, and trees with flowers, which are referred to as "AUT", "SPR w/o f", and "SPR w/ f", respectively. We use our proposed parameter resetting mechanism to adapt to this dynamic. Figure 12 illustrates the received signal power and ESP estimation error for the three foliage density statuses. Figure 12(a) indicates that foliage density significantly impacts the received signal power. *FLog* handles foliage density variations by continuous parameter refitting scheme. In particular,

(a) ESP *vs.* season

(b) ESP error *vs.* season
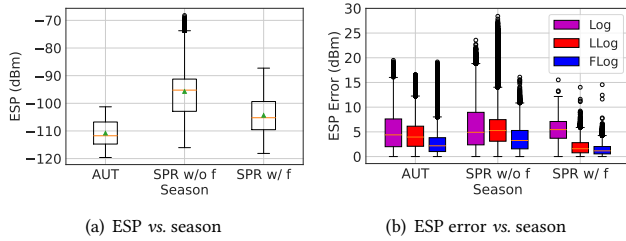
Figure 12: The impact of the environmental dynamic (3): foliage density changes.

(a) ESP *vs.* distance

(b) ESP error distribution
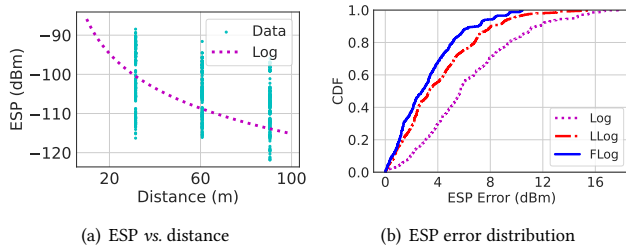
Figure 13: The impact of the environmental dynamic (4): long-term foliage shape changes.

Figure 12(b) shows that *FLog* is capable of adapting well to this dynamic, with estimation errors of 2.85, 3.61, and 1.42 dBm across three foliage density states.

Environmental Dynamics (4): long-term foliage shape changes. We collected data at another almond orchard to evaluate the impact of different growing conditions on our proposed method, which we refer to as environmental dynamic (4). The transmission settings of the nodes were the same as those used in the testbed, and we collected data at three communication distances with seven different directions (0°, 15°, 30°, 45°, 60°, 75°, and 90°). We used the fitted parameters from the testbed data to estimate the link quality in the new orchard. To reconstruct the 3D structure, *FLog* requires measuring one tree, as described in Section 4.4. The new 3D structure will be used to calculate P_{open}, $P_{foliage}$ in Equation (6).

The results, shown in Figure 13, indicate that *FLog* achieved an average estimation error that was reduced by 48.3% and 16.2%, compared to Log and LLog, respectively. Figure 13(a) shows that the Log model could roughly fit the measured signal over the communication distance. However, *FLog*'s performance was comparable to the overall performance reported in Section 5.2, with an average ESP of 2.51 dBm compared to 3.42 dBm for Log. This confirms that *FLog* is insensitive to different almond fields and growing conditions.

Figure 13(b) illustrates that LLog achieved a similar ESP error to *FLog*. This could be attributed to the smaller shape of trees in this orchard, and LLog generates a smaller shadowing media portion, closer to that of *FLog*. The statistics indicate that the two methods had comparable estimations of $P_{foliage}$, averaging 0.17 and 0.24. Hence, LLog delivers a performance comparable to *FLog*.

5.3 Generalizability of *FLog*

The results of the aforementioned experiment demonstrate the effectiveness of our model in almond orchards. We also conducted

(a) ESP *vs.* distance

(b) ESP error distribution
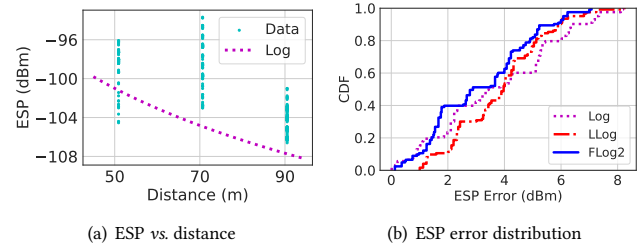
Figure 14: The impact of the orchard species.

further studies to evaluate the performance of our system under various experimental settings, including different orchard species, different gateway, and sensor heights. It's worth noting that the collected data was solely used to test all models with parameters that were fitted from previous fitting data.

5.3.1 Impact of Orchard Species. Since different types of orchards may exhibit varied shadowing effects, it is intuitive to have different β values for other species. Given that walnut trees share a relatively different foliage shape and density with almonds, we chose it to evaluate the generalizability of *FLog*.

To fit parameters in a walnut orchard, we collected data at a horizontal distance of 50 m and 90 m in three directions (30°, 60°, and 90°). We then utilized three path loss models with newly fitted parameters to estimate the link quality in the same walnut orchard, the evaluation is conducted on the data collected at 70 m in three different directions (30°, 60°, and 90°). All other transmission settings remained the same as the testbed.

As shown in Figure 14(a), similar trends were observed in the walnut orchard as in the almond orchard, *i.e.*, the ESP of the received signal decreased with increasing communication distance. Figure 14(b) reports the CDF of the ESP estimation error for different models, which shows that *FLog* provides the highest estimation accuracy. Specifically, *FLog* reduced the error by 15.4% and 18.0% for the Log and LLog models, respectively.

5.3.2 Impact of Transmission Parameters. To evaluate the robustness of *FLog*, we conducted controlled experiments to study the effects of various parameters on our model. Theoretically, transmission power, antenna gain, frequency, and SF do not have a direct impact on the path loss exponent, which is what the link quality models aim to estimate. The packet size may slightly affect the calculation of SNR on the hardware and thus lead to a variation in ESP. Figure 15 and Figure 16(a) shows the estimation error for different SFs, frequency bands, and packet sizes, and the results demonstrate that none of these parameters have a significant effect on the ESP.

5.3.3 Impact of Sensing Cycle. We utilize the most recently received N packets to perform the parameter resetting mechanism, where N is set to 5. The performance of this mechanism may be influenced by the sensing cycle, which is the time between two adjacent transmitted packets. In our testbed, each node sends 45 packets every 15 minutes with a 20-second interval. To simulate a 15-minute sensing cycle, we use the first, 46th, 91st, 136th, and 181st packets to recalibrate our model's parameters, which are then

(a) ESP error *vs.* SF

(b) ESP error *vs.* frequency
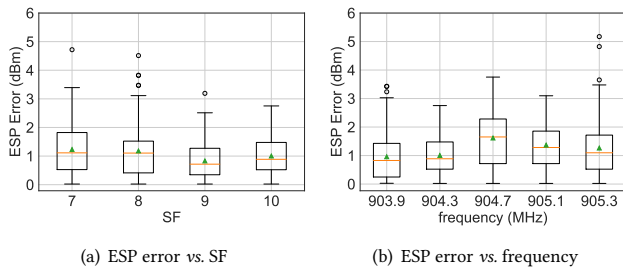
Figure 15: The impact of SF and frequency.

(a) ESP error *vs.* packet size

(b) ESP error *vs.* sensing cycle
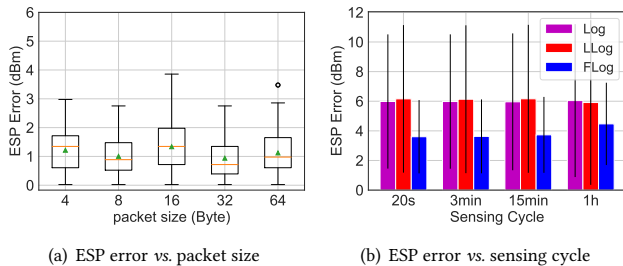
Figure 16: The impact of packet size and sensing cycle.

used to predict the link quality of the 226th packet. This allows us to employ our parameter resetting mechanism at different sensing cycles. Figure 16(b) shows the error bars with different sensing cycles for three models, depicting the standard deviation from the average. We can find that the duration of the sensing cycle has a minimal impact on the performance of our model. Specifically, compared to a sensing cycle of 20 s, the estimation errors of *FLog* increase by 0.87%, 4.03%, and 9.56% with sensing cycles of 3 min, 15 min, and 1 hour. Figure 17 illustrates the received signal power over a period of four weeks. It can be observed that the link quality at a particular location in the orchards remains relatively consistent, indicating that changing the sensing cycle has minimal impact on the estimation error.

It should be noted that for node #1, there were two significant changes in ESP at packet indexes 4,316 and 8,633, respectively. The first change occurred due to a gusty wind that caused the waterproof cover behind the antenna to lift up like a reflection mirror, resulting in a significant increase in ESP. The cover was manually recovered at the second change point, which caused the ESP to return to normal levels. Although this incident caused an increase in errors, its impact on the comparison between different sensing cycles is negligible. This is because two outliers would only affect five estimations in our parameter resetting mechanism. Secondly, during the last week of the four-week period, almond trees began to bloom with flowers, resulting in a significant decrease in the received LoRa signal power for all four nodes, starting from the packet index of 12,952.

5.4 Gateway Coverage Estimation

In this section, we evaluate the ESP estimation error using newly collected data from a new almond orchard. To estimate the gateway coverage, we collected data in a new manner as illustrated
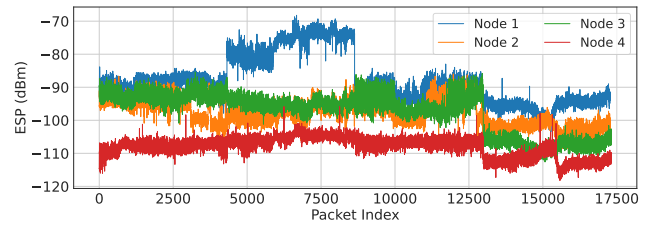
Figure 17: The received signal power at four nodes over a period of four weeks in the temporal dimension dataset.
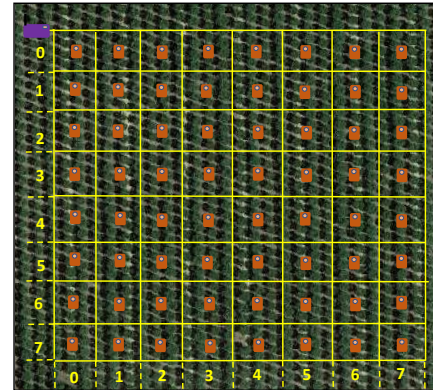
Figure 18: The illustration of collecting data in a new almond orchard for the gateway coverage estimation.

in Figure 18. The orchard was divided into multiple grids with an equal size of 19.2 m × 19.2 m, resulting in a total of 8 × 8 grids. The transmission settings were kept the same as in the testbed. We collected 40 packets at each grid and used the average ESP of the received 40 packets as the ESP ground truth.

ESP Estimation. Figure 19(a) displays the average ESP measurements at each grid, demonstrating that ESP decreases as communication distance increases. To predict ESP values, we used the fitted parameters for the three models in the testbed. Figures 19(b-d) depicts the estimated ESP with Log, LLog, and *FLog* models. The Log model typically underestimates ESP, producing a darker blue, whereas the LLog model tends to overestimate ESP, resulting in a lighter blue. The generated ESP map using *FLog* is the most similar to the ground truth, indicating the lowest ESP estimation error.

PDR Estimation. PDR can be used as an indicator of the gateway coverage map. If PDR is greater than 80% [53, 56], we consider the grid to be covered by the gateway for a specific SF. We also compute the groundtruth of the PDR in each grid by dividing the number of correctly received packets by the total number of sent packets.

The results show that SF7 can cover a large portion of the grids with a PDR of 100%. *FLog* achieves the average estimation error of 0.14, significantly lower than 0.26 and 0.46 of Log and LLog. Log underestimates the ESP of the received signal, ending up estimating that only eight grids can be covered, while LLog overestimates the received ESP, predicting that the gateway can cover almost all grids.

Reducing Construction Cost of Gateways. Given the cost of building a gateway with a height of 10 m consuming $15,400,

(a) ESP groundtruth   (b) Log model   (c) LLog model   (d) *FLog* model
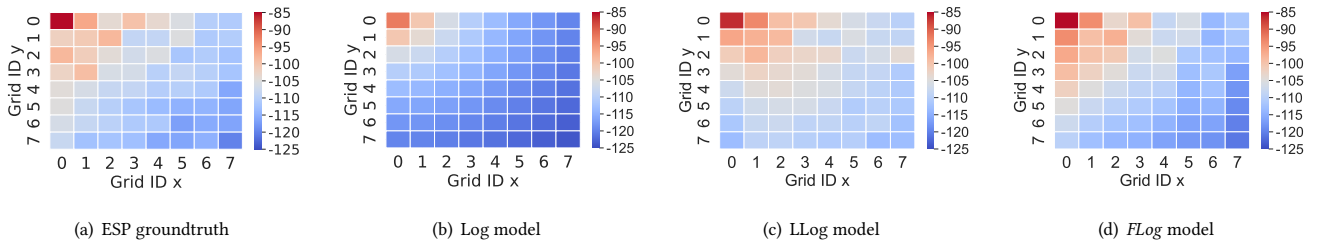
Figure 19: The ESP groundtruth and prediction results of three models on an almond orchard with 8×8 grids.

(a) PDR groundtruth   (b) Log model   (c) LLog model   (d) *FLog* model
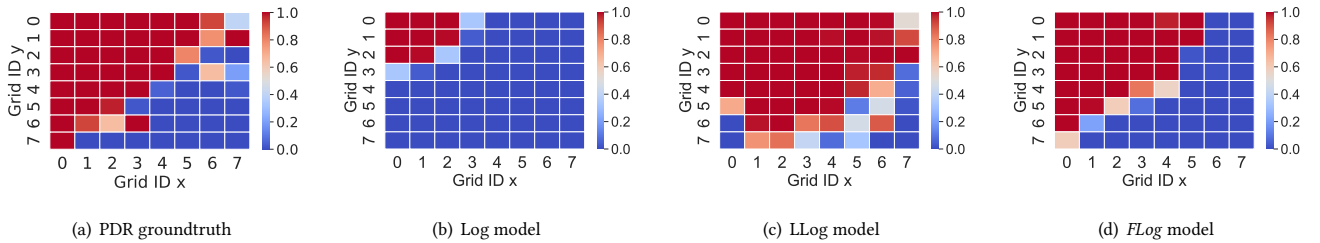
Figure 20: The measured PDRs and corresponding PDRs predicted by three propagation models in an almond orchard.

building fewer gateways while maintaining reliable link quality would be advantageous. We use the above almond orchard with a 10-acre orchard as an example. *FLog* suggests only two gateways with a height of 10 m to cover all nodes and it ends up with communication failure. In contrast, Log suggests using seven gateways, which would increase the cost of building gateways to 107,800 dollars. On the other hand, LLog suggests using only one gateway, but with communication failure in approximately 20% of the area. Such failures can lead to water waste or yield drop, negatively affecting the performance of many smart agricultural applications [11, 25].

6 RELATED WORK

Modeing LoRa Link Quality. There have been numerous empirical studies conducted on the LoRa link quality [5, 6, 8, 10, 13, 21–23, 29, 34, 38, 42, 50]. Adrian *et al.* [54] select locations of sensors and gateways to provide an LoS signal propagation path in FFZ. *FLog* models LoRa link quality in orchards by taking into account shadowing features in a fine-grained manner using FFZ. Silvia *et al.* [10] utilize remote sensing to quantitatively analyze the composition of land covers along LoRa links. Based on the dominant land-cover type along the link, they decide the right version of the Okumura-Hata model from two variants [20, 32, 37]. However, their method is not applicable in orchard scenarios for two reasons. 1) Since orchards typically only have one type of land cover (*i.e.*, trees), their method will ignore local spatial shadowing features such as the amount of space blocked by trees between the sensor nodes and the gateway. 2) The Urban model has deterministic parameters that are empirically fitted for cellular signals, which are typically received by base stations with high antenna heights, unlike LoRa gateways used in orchards.

Extensive measurements [5, 13, 21, 23, 50] have been conducted in various environments, such as indoor, urban, rural, and multi-floor buildings. Based on these measurements, empirical path loss models have been derived. Although these models have a good performance on the collected data, they do not consider the unique features of orchards, e.g., large deviations of the received signal powers in different directions. In contrast, *FLog* is a model based on FFZ theory, which can capture the wireless signal propagation mediums in orchards through 3D modeling.

Foliage Effect on Wireless Signals. It has been found that foliage can significantly affect link quality [24]. Several empirical foliage loss models have been proposed, such as the Weissberger model [46], ITU Recommendation (ITU-R) model [4], and COST235 model [19]. However, using these models in orchards is challenging due to three reasons. Firstly, they use wireless signals with different frequency bands, leading to different attenuation. Secondly, most of these models are deterministic, without adjustable parameters to adapt to different orchards. Thirdly, they cannot handle large deviations of signal power in different directions. In contrast, our system, *FLog*, estimates link quality by considering the surrounding trees and free space within the FFZ.

7 CONCLUSION

This paper presents *FLog*, a propagation model for LoRa signals in orchards. We first investigated the propagation characteristics of LoRa signals in orchards, revealing strong diffraction caused by trees and the ground. To capture these features, *FLog* estimates link quality by calculating the PLE in the Log-Normal Shadowing model for any pair of nodes and gateway using the FFZ theory. Extensive experiments demonstrate the effectiveness of our model.

REFERENCES

[1] 2017. LoRa Packet Logger. https://github.com/Lora-net/lora_gateway.
[2] 2020. Semtech SX1276 datasheet. https://www.semtech.com/products/wireless-rf/lora-transceivers/sx1276.
[3] 2021. Arduino Uno Rev3. https://store-usa.arduino.cc/products/arduino-uno-rev3/?selectedStore=us.
[4] CCIR XVth Plenary Assembly. 1982. Influence of terrain irregularities and vegetation on tropospheric propagation.
[5] Said Benaissa, David Plets, Emmeric Tanghe, Jens Trogh, Luc Martens, Leen Vandaele, Leen Verloock, Frank AM Tuyttens, Bart Sonck, and Wout Joseph. 2017. Internet of animals: characterisation of LoRa sub-GHz off-body wireless channel in dairy barns. *Electronics Letters* 53, 18 (2017), 1281–1283.
[6] Martin C. Bor, Utz Roedig, Thiemo Voigt, and Juan M. Alonso. 2016. Do LoRa Low-Power Wide-Area Networks Scale?. In *ACM MSWiM*.
[7] Marco Cattani, Carlo Alberto Boano, and Kay Römer. 2017. An experimental evaluation of the reliability of LoRa long-range low-power wireless communication. *Journal of Sensor and Actuator Networks* 6, 2 (2017), 7.
[8] Marco Centenaro, Lorenzo Vangelista, Andrea Zanella, and Michele Zorzi. 2016. Long-range communications in unlicensed bands: The rising stars in the IoT and smart city scenarios. *IEEE Wireless Communications* 23, 5 (2016), 60–67.
[9] Tuan Dang, Trung Tran, Khang Nguyen, Tien Pham, Nhat Pham, Tam Vu, and Phuc Nguyen. 2022. ioTree: a battery-free wearable system with biocompatible sensors for continuous tree health monitoring. In *ACM MobiCom*.
[10] Silvia Demetri, Marco Zúñiga, Gian Pietro Picco, Fernando Kuipers, Lorenzo Bruzzone, and Thomas Telkamp. 2019. Automated estimation of link quality for LoRa: A remote sensing approach. In *ACM/IEEE IPSN*.
[11] Xianzhong Ding and Wan Du. 2022. DRLIC: Deep Reinforcement Learning for Irrigation Control. In *ACM/IEEE IPSN*.
[12] Wan Du, Jansen Christian Liando, Huanle Zhang, and Mo Li. 2015. When pipelines meet fountain: Fast data dissemination in wireless sensor networks. In *ACM SenSys*.
[13] Rida El Chall, Samer Lahoud, and Melhem El Helou. 2019. LoRaWAN network: Radio propagation models and performance evaluation in various environments in Lebanon. *IEEE Internet of Things Journal* 6, 2 (2019), 2366–2378.
[14] Tallal Elshabrawy and Joerg Robert. 2018. Closed-form approximation of LoRa modulation BER performance. *IEEE Communications Letters* 22, 9 (2018), 1778–1781.
[15] Amalinda Gamage, Jansen Christian Liando, Chaojie Gu, Rui Tan, and Mo Li. 2020. LMAC: Efficient carrier-sense multiple access for LoRa. In *ACM MobiCom*.
[16] Weifeng Gao, Wan Du, Zhiwei Zhao, Geyong Min, and Mukesh Singhal. 2019. Towards energy-fairness in LoRa networks. In *IEEE ICDCS*.
[17] Orestis Georgiou and Usman Raza. 2017. Low power wide area network analysis: Can LoRa scale? *IEEE Wireless Communications Letters* 6, 2 (2017), 162–165.
[18] Xiuzhen Guo, Longfei Shangguan, Yuan He, Nan Jing, Jiacheng Zhang, Haotian Jiang, and Yunhao Liu. 2022. Saiyan: Design and Implementation of a Low-power Demodulator for LoRa Backscatter Systems. In *USENIX NSDI*.
[19] MPM Hall. 1993. COST project 235 activities on radiowave propagation effects on next-generation fixed-service terrestrial telecommunication systems. In *IET ICAP*.
[20] Masaharu Hata. 1980. Empirical formula for propagation loss in land mobile radio services. *IEEE transactions on Vehicular Technology* 29, 3 (1980), 317–325.
[21] Salaheddin Hosseinzadeh, Hadi Larijani, Krystyna Curtis, Andrew Wixted, and Amin Amini. 2017. Empirical propagation performance evaluation of LoRa for indoor environment. In *IEEE INDIN*.
[22] Oana Iova, Amy L Murphy, Gian Pietro Picco, Lorenzo Ghiro, Davide Molteni, Federico Ossi, and Francesca Cagnacci. 2017. LoRa from the city to the mountains: Exploration of hardware and environmental factors. In *ACM EWSN*.
[23] Pascal Jörke, Stefan Böcker, Florian Liedmann, and Christian Wietfeld. 2017. Urban channel models for smart city IoT-networks based on empirical measurements of LoRa-links at 433 and 868 MHz. In *IEEE PIMRC*.
[24] MS Karaliopoulos and F-N Pavlidou. 1999. Modelling the land mobile satellite channel: A review. *Electronics & communication engineering journal* 11, 5 (1999), 235–248.
[25] Abhishek Khanna and Sanmeet Kaur. 2019. Evolution of Internet of Things (IoT) and its significant impact in the field of Precision Agriculture. *Computers and electronics in agriculture* 157 (2019), 218–231.
[26] Chenning Li, Hanqing Guo, Shuai Tong, Xiao Zeng, Zhichao Cao, Mi Zhang, Qiben Yan, Li Xiao, Jiliang Wang, and Yunhao Liu. 2021. NELoRa: Towards Ultra-low SNR LoRa Communication with Neural-enhanced Demodulation. In *ACM SenSys*.
[27] Jansen C Liando, Amalinda Gamage, Agustinus W Tengourtius, and Mo Li. 2019. Known and unknown facts of LoRa: Experiences from a large-scale measurement study. *ACM Transactions on Sensor Networks* 15, 2 (2019), 1–35.
[28] Yuxiang Lin, Wei Dong, Yi Gao, and Tao Gu. 2021. Sateloc: A virtual fingerprinting approach to outdoor LoRa localization using satellite images. *ACM Transactions on Sensor Networks (TOSN)* 17, 4 (2021), 1–28.

[29] Li Liu, Yuguang Yao, Zhichao Cao, and Mi Zhang. 2021. DeepLoRa: Learning accurate path loss model for long distance links in LPWAN. In *IEEE INFOCOM*.
[30] Michael Marcus and Bruno Pattan. 2005. Millimeter wave propagation: spectrum management implications. *IEEE Microwave Magazine* 6, 2 (2005), 54–62.
[31] Han Na and Thomas F Eibert. 2022. A Huygens' Principle Based Ray Tracing Method for Diffraction Calculation. In *IEEE EuCAP*.
[32] Yoshihisa Okumura. 1968. Field strength and its variability in VHF and UHF land-mobile radio service. *Rev. Electr. Commun. Lab.* 16 (1968), 825–873.
[33] Yao Peng, Longfei Shangguan, Yue Hu, Yujie Qian, Xianshang Lin, Xiaojiang Chen, Dingyi Fang, and Kyle Jamieson. 2018. PLoRa: A passive long-range data network from ambient LoRa transmissions. In *ACM SIGCOMM*.
[34] Juha Petajajarvi, Konstantin Mikhaylov, Antti Roivainen, Tuomo Hanninen, and Marko Pettissalo. 2015. On the coverage of LPWANs: range evaluation and channel attenuation model for LoRa technology. In *IEEE ITST*.
[35] Michele Preti, François Verheggen, and Sergio Angeli. 2021. Insect pest monitoring with camera-equipped traps: strengths and limitations. *Journal of pest science* 94, 2 (2021), 203–217.
[36] John G.. Proakis and Masoud Salehi. 2008. *Digital communications, 5th edition*. McGraw-Hill.
[37] Theodore S Rappaport et al. 1996. *Wireless communications: principles and practice*. Vol. 2. prentice hall PTR New Jersey.
[38] Yidong Ren, Li Liu, Chenning Li, Zhichao Cao, and Shigang Chen. 2022. Is lorawan really wide? fine-grained lora link-level measurement in an urban environment. In *IEEE ICNP*.
[39] Scipy. [n. d.]. Non-linear Least-Square Algorithm. https://docs.scipy.org/doc/scipy/reference/generated/scipy.optimize.least_squares.html.
[40] Richard L Snyder. 1984. California irrigation management information system. *American potato journal* 61 (1984), 229–234.
[41] Tossaporn Srisooksai, Kamol Kaemarungsi, Junichi Takada, and Kentaro Saito. 2019. Path loss measurement and prediction in outdoor fruit orchard for wireless sensor network at 2.4 GHz band. *Progress In Electromagnetics Research C* 90 (2019), 237–252.
[42] Jothi Prasanna Shanmuga Sundaram, Wan Du, and Zhiwei Zhao. 2019. A survey on LoRa networking: Research problems, current solutions, and open issues. *IEEE Communications Surveys & Tutorials* 22, 1 (2019), 371–388.
[43] Saul A Torrico, Henry L Bertoni, and Roger H Lang. 1998. Modeling tree effects on path loss in a residential environment. *IEEE Transactions on Antennas and Propagation* 46, 6 (1998), 872–880.
[44] United States Department of Agriculture National Agricultural Statistics Service. 2021. 2021 California Almond Acreage Report. https://www.almonds.com/sites/default/files/2022-04/2021_NASS_Acreage_Report.pdf.
[45] United States Department of Agriculture National Agricultural Statistics Service. 2023. California Agricultural Production Statistics. https://www.cdfa.ca.gov/Statistics/.
[46] Mark A Weissberger. 1982. *An initial critical summary of models for predicting the attenuation of radio waves by trees*. Technical Report. Electromagnetic Compatibility Analysis Center Annapolis MD.
[47] Xianjin Xia, Yuanqing Zheng, and Tao Gu. 2019. FTrack: Parallel decoding for LoRa transmissions. In *ACM SenSys*.
[48] Binbin Xie and Jie Xiong. 2020. Combating interference for long range LoRa sensing. In *ACM SenSys*.
[49] Jie Xiong, Karthikeyan Sundaresan, and Kyle Jamieson. 2015. Tonetrack: Leveraging frequency-agile radios for time-based indoor wireless localization. In *ACM MobiCom*.
[50] Weitao Xu, Jun Young Kim, Walter Huang, Salil S Kanhere, Sanjay K Jha, and Wen Hu. 2019. Measurement, characterization, and modeling of LoRa technology in multifloor buildings. *IEEE Internet of Things Journal* 7, 1 (2019), 298–310.
[51] Kang Yang and Wan Du. 2022. LLDPC: A Low-Density Parity-Check Coding Scheme for LoRa Networks. In *ACM SenSys*.
[52] Kun Yang, Andreas F Molisch, Torbjörn Ekman, Terje Røste, and Marion Berbineau. 2019. A round earth loss model and small-scale channel properties for open-sea radio propagation. *IEEE Transactions on Vehicular Technology* 68, 9 (2019), 8449–8460.
[53] Jennifer Yick, Biswanath Mukherjee, and Dipak Ghosal. 2008. Wireless sensor network survey. *Computer networks* 52, 12 (2008), 2292–2330.
[54] Adrian Zarnescu, Razvan Ungurelu, Mihai Secere, Gaudentiu Varzaru, and Bogdan Mihailescu. 2020. Implementing a large LoRa network for an agricultural application. In *IEEE EE&AE*.
[55] Fusang Zhang, Zhaoxin Chang, Jie Xiong, Rong Zheng, Junqi Ma, Kai Niu, Beihong Jin, and Daqing Zhang. 2021. Unlocking the beamforming potential of LoRa for long-range multi-target respiration sensing. *Proceedings of the ACM on Interactive, Mobile, Wearable and Ubiquitous Technologies* 5, 2 (2021), 1–25.
[56] Jerry Zhao and Ramesh Govindan. 2003. Understanding packet delivery performance in dense wireless sensor networks. In *ACM SenSys*.